3-D VSP: Survey design and processing

Qi Zhang, Robert R. Stewart and Zandong Sun

ABSTRACT

This paper studies the design of 3-D VSP surveys. It also outlines a processing procedure to create 3-D images. Two numerical models (a dipping layer and a dome model) are used to test the effects of variable shot and receiver positions. We find that a high fold can be achieved near the well for realistic shot and receiver distributions. In addition, we evaluate an synthetic data the 3-D VSP coverage of a current 3C-3D seismic survey. A 3-D processing flow which includes NMO correction, muting, binning and stack makes excellent images of the targets.

INTRODUCTION

There is often a need for a high-resolution, three-dimensional (3-D) seismic picture around the borehole. Both 3-D VSP (using an areal distribution of surface sources and a downhole tool) and 3-D reverse VSP (with a surface array of receivers and downhole source) hold great promise for near-well imaging.

In situ seismic measurements (VSP, reverse VSP and crosswell surveys) have proven useful for imaging and estimating rock properties near or between wells. However, because the earth is generally heterogeneous in three dimensions and our regions of interest are usually volumetric, 3-D images are critical. Economical surveys are also essential. Thus we must pursue practical measurements which provide 3-D images in a cost-effective way with minimal production impact. We would argue that the 3-D VSP is the current best candidate to solve this problem. Furthermore, the 3-D VSP can piggyback on a conventional 3-D surface seismic survey by passive and simultaneous monitoring of the surface shots. The reverse VSP could also be co-recorded into the 3-D surface geophones, if there were an acceptable downhole source and if its shooting didn't slow the surface survey down too much. There is considerable practice of and literature on 2-D VSP surveying. In addition, a number of authors have recently considered the analysis of 2-D RVSP data (Jackson et al., 1989; Jones, 1991; Kragh et al., 1991; Naville et al., 1991; Hardage, 1992; Parra and Bangs, 1992). Haldorsen et al. (1992) used several 2-D surface lines to image data recorded from a downhole drill-bit source. Their drill-bit seismic image matched surface seismic and conventional walkaway VSP images reasonably well. Aleotti et al. (1994) also showed drill-bit images (prediction ahead of the bit seismograms) that were similar to synthetic seismograms produced from logs after the well had been drilled through the predicted depths. Less has been written on 3-D VSP. Chen and McMechan (1992) considered the 3-D case and used synthetic data from a salt structure model to perform a 3-D pre-stack depth migration. They showed that 2-D analysis produced artifacts while the 3-D algorithms provided a much more accurate picture.

In this work, we address the survey design issues of 3-D VSP via a 3-D VSP CDP binning procedure. We also propose procedures for handling and processing of model and field 3-D VSP data. In this numerical modeling paper, we will not distinguish between VSP and reverse VSP procedures.

NUMERICAL MODELING EXAMPLES

Two numerical datasets are used here. The first data set was generated from model A which consists of three layers with reflections from all three layers. The East-West cross section of the model is shown in Figure 1a. The thicknesses of the three layers from top to bottom are 800 m, 400 m (at the well location, dipping layer), 800 m respectively. The acquisition parameters are listed as follow in Table 1:

<u>Table 1. 3-D VSP modelling parameters</u>

Receiver line spacing: 50 m 61 receivers per line.

Receiver line orientation: East-West

Receiver line length 3000 m

Receiver spacing: 50 m

Well location: centre of model (1500 m,1500 m)

Source spacing: 40 m (in borehole from 1200 m to 0 m)

Wavelet: 50 Hz Ricker wavelet

Shot gather: 3600 traces/record

Data set B is from a previous study (Sun and Stewart, 1994). The model consists of three layers (Figure 1b). The thicknesses of the three layers from top to bottom are 800 m, 400 m and 800 m respectively. A dome centered at (1500m, 1500m) is located on the top of the second layer with a radius of 630 m and height of 210 m, which possesses dip angles varied from 0˚ to 36.9˚. The dataset was generated with reflections only from bottoms of the first layer (dome structure) and second layer.

The source and receiver geometry configuration of both datasets are the same, and are shown in Figure 2. The examples of raw records of both shots gathers and receiver gathers are shown in Figure 3.

3-D VSP PROCESSING

There are a number of steps required to process 3-D VSP data, some of them have been previously addressed (Sun and Stewart, 1994), for example, wavefield separation using a velocity filter or median filter. Our discussion in this paper will center on NMO correction, binning and stacking.

Normal moveout (NMO) correction, binning and stacking

The offset VSP survey is used to create reflection points which are laterally offset from the borehole. Using a ray parameter approach, Stewart (1991) developed an algorithm for 2-D P-P and P-S offset VSP mapping. These mapping techniques are extended to the 3-D case. The mapping technique for 3-D RVSP data can be used for 3-D VSP data by exchanging source-receiver geometry information.
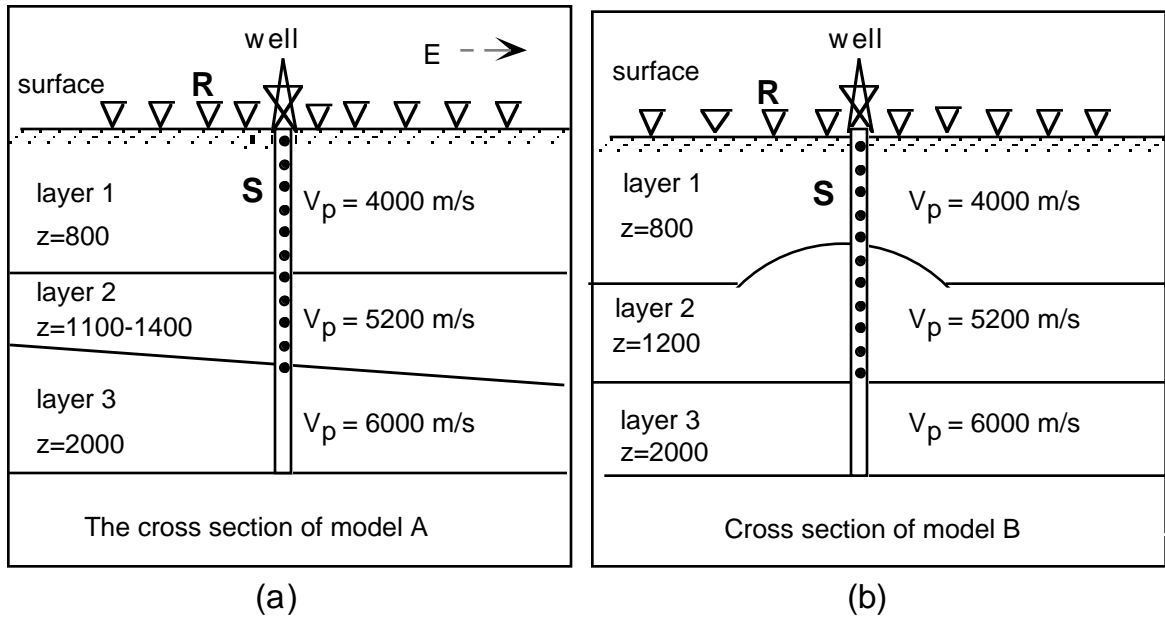
FIG. 1 Cross section of models A and B; dipping and domed structures
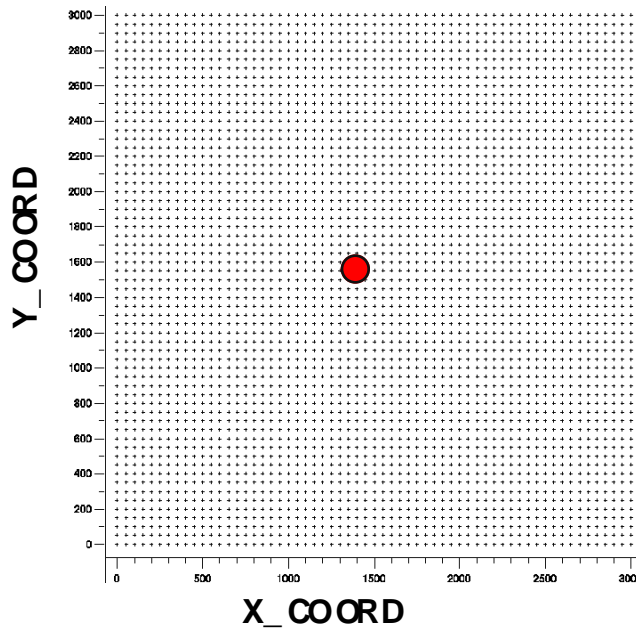

FIG. 2. Surface receiver layout geometry (61 receiver lines with a 50 m line spacing and 61 receivers on each line with 50 m receiver spacing). The well location is shown as a dot in the centre of the receivers area.
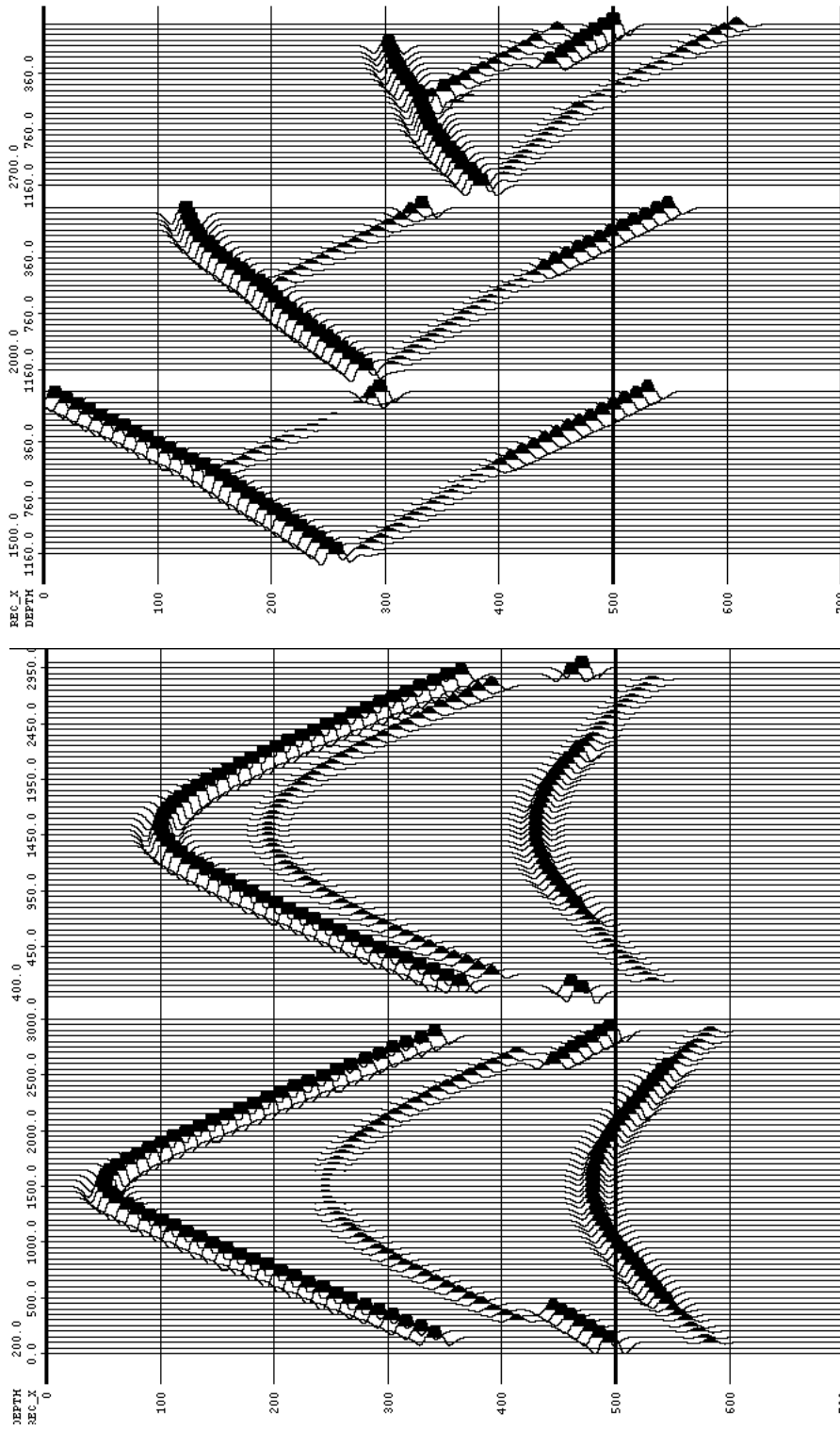
FIG. 3. Raw synthetic records from model B. (a): Shot gathers (from shot depths of 200 m and 400 m) at crossline 1500m ; (b): Receiver gathers at crossline 1500m, (at stations 1500m, 2000 m and 2700 m) for shots at depths from 1600 m to the surface.

In the 2-D case, the lateral offset of the reflection point X_r (in Figure 4a) is given by:

$$X_r = \frac{X}{1 + \dfrac{\widetilde{V_R}^2 T_R}{\widetilde{V}_{RB}^2 T_{RB}}} , \tag{1}$$

where $\widetilde{V}_R$ is the RMS velocity of upgoing raypath or downgoing raypath , $\widetilde{V}_{RB}$ is the RMS velocity for downgoing raypath or upgoing raypath, T_R is the zero-offset traveltime (one way) from surface to reflection point; and T_{RB} is the zero-offset traveltime (one way) from reflection point to borehole a source (for RVSP) or a receiver (for VSP). X is the source-receiver offset.

The concept used to calculate the reflection point of 3-D VSP is diagrammed in Figure 4. The reflection point denoted by C in Figure 4(b) is in the xy plane instead of in x direction only .The reflection point is located in the propagation plane of the P wave. We can define the azimuth of the reflection point by calculating the source-receiver line azimuth angle θ with the X or Y axis; then θ is written as

$$\theta = \tan\left(\frac{\Delta Y}{\Delta X}\right)^{-1} \tag{2}$$

where ΔX and ΔY are the horizontal offsets from the well top in the y and x direction.

Extending equation (1) to the 3-D domain, gives:

$$R_{offset} = \frac{\sqrt{\Delta X^2 + \Delta Y^2}}{1 + \dfrac{\widetilde{V}_R^2 T_R}{\widetilde{V}_{RB}^2 T_{RB}}} , \tag{3}$$

where ΔX and ΔY are the horizontal offset from the surface location to the well top in the y and x direction.

The horizontal distance covered by the reflected wave in the x direction is given by

$$X_r = R_{offset}\sin(\theta) \tag{4}$$

The horizontal distance covered by the reflected wave in the y direction is given by

$$Y_r = R_{offset}\cos(\theta) \tag{5}$$

Equation (3) provide the binning method. Once we calculate the coverage of the reflection point by using equation (3), we can split it into the x and y axes by using equations (4) and (5).

Since the shots are in a two dimension plane, the 3-D VSP has the character of surface 3-D seismic data. Therefore, it is necessary to define the bin grid in two dimensions as in surface 3-D data binning. This is shown in Figure 5a. On the other hand, the receivers in the well borehole, the 3-D VSP also has the character of VSP seismic in which is the reflection points for each recorded trace are variant in depth

domain as shown in figure 5b. If we define the same bin origin and grids in 2-D plane for all depth layers of interests, for same trace at different depth points, the reflection points will be located in different bin cell.

By combining the two characters of 3-D VSP, the bin grids are defined in a two dimensional plane, and the reflection points are calculated in 2-D plane at each depth point by using equations (3) to (5) and the reflection points of the 3-D VSP are mapped in 3-D position.
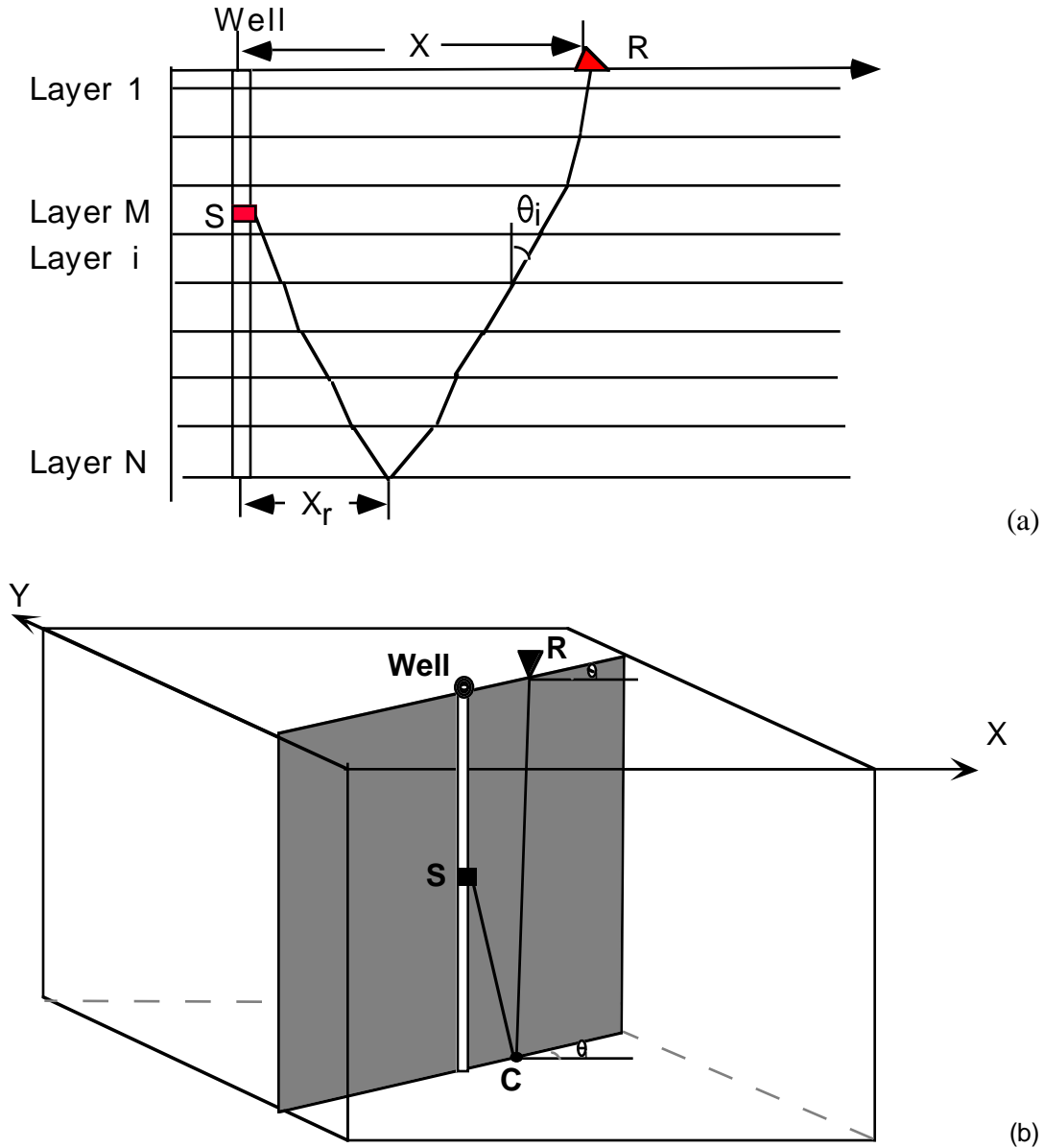

(a)

(b)

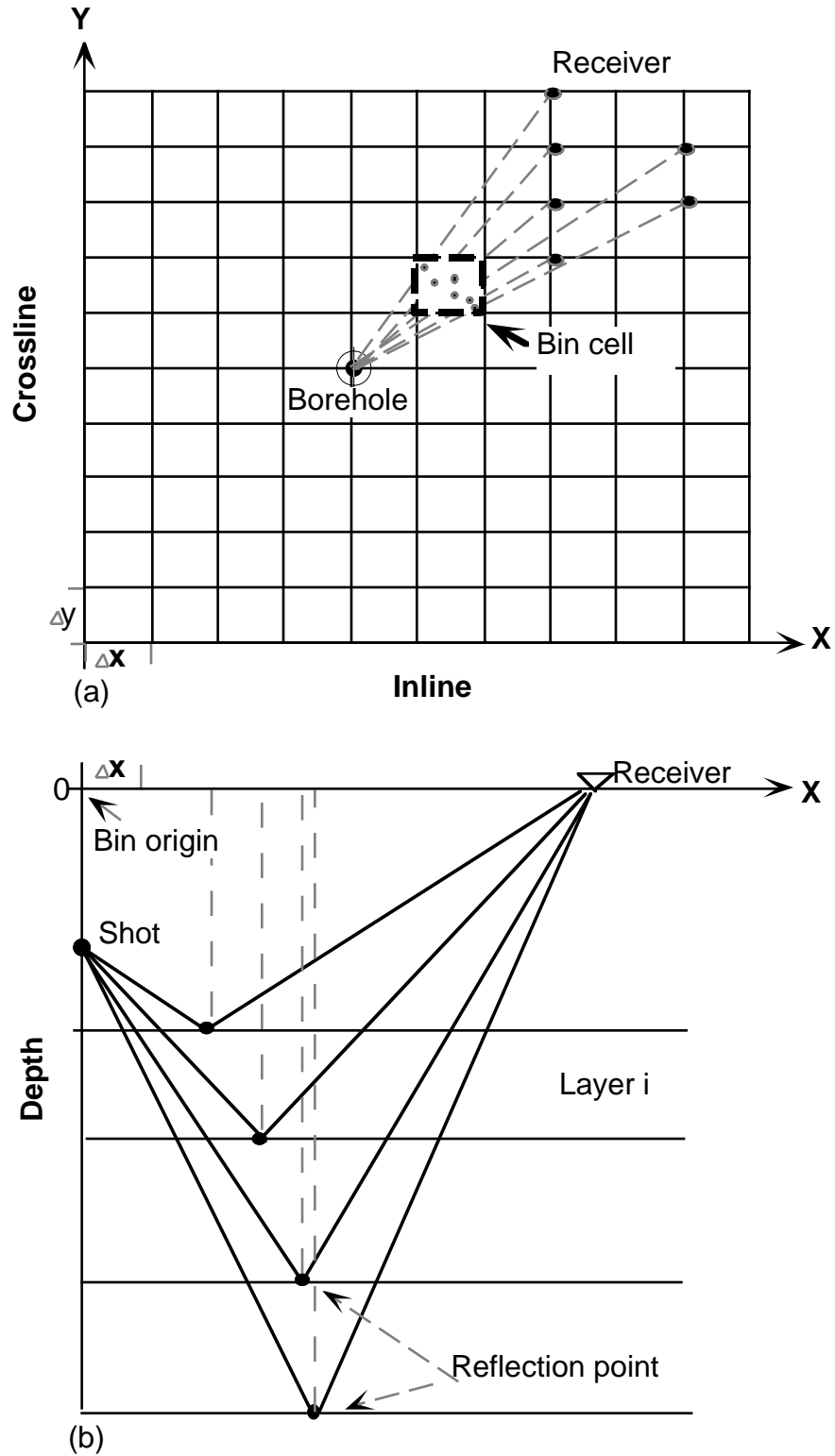FIG. 4. VSP ray geometry for a flat horizontally layered medium , (a): 2-D case; (b): 3-D case.

FIG. 5. Schematic diagram showing binning algorithm. (a) surface diagram; (b): depth domain diagram

3-D VSP fold distribution

For reflection imaging, the stacking fold or multiplicity, is a critical parameter. In this study, we have done several tests on model A, in order to learn how the surface geometry and down hole operation influence the bin interval and the fold distribution.

Figures 6 and 7 are used to illustrate the binfold distribution as depth (time) increases. These two results are the binning algorithm performed on the same dataset where the inline and crossline receiver coordinates are from 200 to 2800 meters, the inline and crossline receiver intervals are 50 meters. There are 30 shots located at the surface 1500 m in both directions, and located from surface down to the well to borehole 1200 m with depth interval 30 meters. All the shots are above (one is on) the second layer in the model A, which means the results in Figure 6 and 7 based on the same surface and depth geometry.

We use same bin interval, azimuth and bin origin on these layers. the bin origin and azimuth are the same as surface layout coordinate origin and azimuth. the bin interval in both directions is 15 m.

Figure 6 shows the areal bin fold distribution (Figure 6a) around 600 ms (the reflection of the second layer in model A). The bin fold statistics are shown in the histogram (Figure 6b). The overall the fold distribution is not quite uniform. Two "black" strips across the covered area East-West and North-South through the Well with low fold coverage (from 3 fold to 40 fold) along which higher fold coverage (60 to 70 fold) are surrounded (Figure 6a). Two "bright" strips across the covered area through the Well 45° from any of the "black" strips with high fold coverage (80 to 100 fold).The dominant coverage is about 50 to 60 fold but they are distributed in the 45° azimuth of receiver line direction. There also have quite big portion of bin cell with low fold (3 to 10) coverage distributed along the first and last 10 inline and crossline. As the depth (time) increases, the bin fold distribution gets more uniform as illustrated in Figure 7. As in figure 6, there are two "black" strips across the well top in receiver inline and crossline direction. The major fold distribution becomes much more uniform and this also can be viewed in figure 7(b),the histogram shows better distribution, and much higher fold. The dominant fold coverage of the third layer is around 40-75 fold, and there is almost no low fold less 35 between 10-80 inline and crossline of CRPs (reference numbers) as displayed in figure 15 except the two "black" strips cross the well top.

Comparing Figures 6 and 7, we find out that as the depth increase the bin fold will distributed more uniformly and is higher than in shallower layers.

Figure 8 shows the bin fold distribution of the same dataset of layer 3 by using same parameters except now shifting the bin origin 7.5 m towards east and north directions. We can see the two "black" strips have disappeared. Figure 9 shows the bin fold distribution of layer 3, the bin size of 30 m in both direction. Comparing Figure 9 and 7, we can see by increasing the bin size, the binfold will distribute more uniformly with high fold.

Figures 10 illustrate the fold distribution when few shots are used. In this Figure, we take out every second shot as shown in Figure 7, giving only 15 shot, They located from the surface down to the well to 1160 m with an 80 m interval. Comparing Figure 10 with Figure 7, we find that the binfold distribution is not much different. The dominate binfold is 22 to 27, which is half amount of its shown in Figure 7. This

indicates that the number of shots or receivers downhole does not strongly influence the fold distributions.

Figure 11 illustrates the fold distribution when the surface geometry changes. In this test, we keep the shot depth and number the same as in Figure 7, but we take out every second receiver in the surface ,giving a receiver interval 100 meters in both inline and crossline. The result in Figure 11 shows the binfold is low and there are lot of zero bins inside the offset 700 meters. This tells us the surface station geometry heavily influences both the bin size and the bin fold.

 Through these tests, we find that the minimum bin size is 1/3 inline interval * 1/3 crossline interval

NMO correction application

The approximate traveltime for 2-D VSP of P-P reflected wave (Stewart 1991) is:

$$t = T_R + T_{RB} + \frac{X^2}{2\left[\tilde{V}_R^2 T_R + \tilde{V}_{RB}^2 T_{RB}\right]} \quad, \tag{6}$$

where $\tilde{V}_R$, $\tilde{V}_{RB}$, T_R and T_{RB} are defined as in equation (1).

Extending equation (6) to the 3-D domain, the traveltime of the P-P reflected wave from the source to the receivers is written as

$$t = T_R + T_{RB} + \frac{\sqrt{\left(\Delta X^2 + \Delta Y^2\right)}^2}{2\left[\tilde{V}_R^2 T_R + \tilde{V}_{RB}^2 T_{RB}\right]} \quad, \tag{7}$$

where ΔX and ΔY are the horizontal offset from the surface location to the well top in y and x direction.

Equation (7) provides the NMO correction method for 3-D VSP wavefield. That is to put the amplitude of seismic wavefield at t time to a two-way normal incidence P-P time (T_R) in two dimensional domain.

 In this paper, the NMO algorithm is performed on two numerical 3-D VSP model datasets. The procedure is shown in Figure 12. The input data is the preprocessed upgoing wave. RMS velocities and the raypath travel time are calculated by using known interval velocity and depth information.

Figure 14 shows some of the upgoing waves of model A and B. Three receiver gathers from each model are located at north-southing 1500 m (cross well top) and east-westing 1500,2000, 2700 meters, the shot depth are from 1200 meters down the borehole up to the surface. The preprocessed upgoing wavefield is the input into the NMO processing flow.

Figure 15 shows some of the results of NMO applied crossline section of model A. Data are sorted in common shot gathers at different surface inline locations and variant shot depths. Figure 15a and 15b are the same shot gather at shot depth at surface, but the inline location of the receivers are located at 1500 meters (at the well top), and 2200

meters (700 meters away from the well top) differently. Comparing these two, we can see as the horizontal offset of receiver increase, the accuracy of NMO correction on the event at the far offset of the shallow layer decrease. Figure 15c is a shot gather located at the some location of figure 15a but the shot depth is 120 meters down the well borehole. Comparing this two, we found out as the shot depth becomes deeper, the error grows bigger. Figure 9d is the inline receiver located at 50 meters away form the well top, but the shot depth at 320 meters down the borehole. This figure have proved the effect at the far offset at the shallow layer.

Figure 16 shows the result of NMO applied on dome model B. The geometry is the same as described (in Figure 15).We can see from this Figure, that the NMO algorithm performed well, except at shallow layer at far offset, the deeper shots depth (320 m in the figure 10d).

Over all, particularly the NMO correction performed well on the deeper layers of both dipping layered model and dome structured model.

NMO correction error discussion

The NMO correction error at far offset at the shallow layer can be explained by viewing equation (7). First, we use equation (7) to calculated the two-way traveltime. This equation assumes that the angle of the raypath with the vertical direction is small. This is true only when the horizontal offset is small comparing with the layer depth of interests. Second, the depth of the tools down the borehole is another parameter effect the NMO traveltime, this is denoted as T_{RB} in equation (6) and (7). When the angle is not small, T_{RB} will be very small at the deeper tool depth and this will exaggerate the error caused by the large offset. In our research, we found that for a the horizontal offset great than 1000 m in our model, NMO correction by using equation (7) will produce a large error at layer depth 800 m down the surface.

Binning and stacking

The binning algorithm is used on both dataset A and B. The flowchart of binning is shown in Figure 13. Since the far offset effects, the input dataset is the NMO applied dataset with NMO stretch mute. Like surface 3-D processing , there are four important parameters for binning algorithm: the maximum coverage in 2-D plane; bin intervals; bin azimuth; and the bin fold. In this study, the maximum offset coverage in calculated as the half of the maximum offset at surface. The bin inline and crossline directions are in the surface inline and crossline directions. The bin interval and the fold will discussed in fallow section.

As discussed above 3-D VSP binning is depth variant. Therefore, we need to calculate RMS velocity and raypath traveltimes, and these are the input parameters of equation (7). In practice, we find out that the bin interval of 15 m for both inline and crossline gave good results. Figure 18 and 19 show some further binning and stacking results.

Figure 18a and 18b are inline common reflection point gather (CRP) stack section (east-west direction) for the dipping layered model A. Figure 18a is the CRP bin located at crossline near offset 1515 meters, which is 15 meters away from the well top horizontally. Figure 18b is the CRP bin located at crossline far offset 1930 meters , which is 430 meters away from the well top. These two figures show that the binning

algorithm performed well. On the first layer (400 ms in time) there is not much data, that is because the error of NMO correction.

Figure 19 shows some of the crossline CRP stack sections. Figure 19a shows the inline CRP bin at 1530 meters, which is 30 meters away from well. Figure 19b shows the inline CRP at 2025 meters, which is 525 meters away from well top. These figures indicated the binning and stacking algorithm works reasonably well.

Figure 20a and 20b show some CRP stacks from model B. Figure 20a is located at inline CRP bin coordinate of 1515 m while 20b is at 1230 m. In areas of high dip there are some mapping errors. This is due to mapping velocity errors and the flat layer assumptions. We expect that the depth migration will migrate the structure to it true location and this will be part of our future work.

CONCLUSIONS

In this study, we have developed a 3-D VSP NMO and binning algorithm. The raypath NMO traveltime performs well when the horizontal offsets were less than 1200 meters for the dipping layered model A, and 1000 meters for structure layered model B at shallow layer. When the offset is too large or the velocity at the shallow layer is too slow, a large error will occur in the mapping.

3-D VSP binning has both characteristics of VSP and surface 3-D seismic.

Surface geometry is used to determine the bin size and bin azimuth. The surface intervals are the major influence on the bin fold. The number of downhole positions is the major parameter for the bin fold. Changing the number of the downhole locations or the tool interval has no much influence on the distribution of the bin fold.

FUTURE WORK

There are numerous aspects of 3-D VSP survey design to investigate. For example, if we have a limited receiver array, where should it be positioned to give the most broad, but uniform fold coverage? In processing, there are many algorithms to adapt to the 3-D VSP case. We need to be able to do velocity analysis (from direct arrivals and reflections) as well as ray trace mapping and prestack migration

ACKNOWLEDGMENTS

REFERENCES

Aleotti, L., Gallori, A., Miranda, F., Craglietto, A., Persoglia, S., Poletto, F., Impact of drill-bit seismic method on exploitative wells: Presented at the **56**th Ann. Mtg., Europ. Assn. Explor. Geophys., Vienna.

Chen, H. and McMechan, G.A., 1992, 3-D pre-stack depth migration for salt and subsalt structures using reverse-VSP data: J. Seis. Expl., **1**, 281-291.

Eaton, W. S. D., Stewart, R. R., and Harrison, M. P., 1991, The Fresnel zone for P-SV waves: Geophysics **56**, 360-364.

Haldorsen, J. B. U., Miller, D. E., Walsh, J. J., and Zoch, H.-J., 1992, Multichannel approach to signature estimation and deconvolution for drill bit imaging: Presented at the **62**nd Ann. Intl. Mtg., Soc. Explor. Geophys., New Orleans.

Hardage, B.A., 1992, Reverse VSP and crosswell seismology: Geophysical Press.

Jackson, P.J., Onions, K.R., and Westerman, A.R., 1989, Use of inverted VSP to enhance the exploration value of boreholes: First Break, **7**, 233-246.

Jardine, D. 1974, Cretaceous oil sands of Western Canada: CSPG Memoir **3**, 50-67.

Jones, M., 1991, On the analysis of a reverse VSP data set using a core-gun source: Presented at the Sixty-First Ann. Intl. Mtg. Soc. Expl. Geophys., Houston.

Labonté, S., 1990, Modal separation, mapping, and inverting three-component VSP data: M.Sc. thesis, University of Calgary.

Kragh, J.E., Goulty, N.R., and Findlay, M.J., 1991, Hole-to-surface seismic reflection surveys for shallow coal exploration: First Break, **7**, 335-344.

Minken, F.D., 1974, The Cold Lake Oil Sands: Geology and a reserve estimate: CSPG Memoir **3**, 84-89.

Naville, C., Layotte, P.C., Serbutoviez, S., and Verdier, F., 1991, Uphole surveys digitally recorded and processed as multi-offset RVSP's: Presented at Ann. Mtg. Europ. Assoc. Expl. Geophys., Paris.

Parra, J. O. and Bangs, J. H., 1992, High-resolution reverse VSP and interwell seismic experiments at the Buckhorn test site in Illinois: Presented at the **62**nd Ann. Intl. Mtg., Soc. Explor. Geophys., New Orleans.

Stewart, R. R., 1991, Rapid map and inversion of P-S waves: Geophysics, **56**, 859-862.

Sun, Z. and Stewart, R. R., 1994, 3-D reverse VSP: CREWES Report, 1994.

Toksöz, M. N. and Stewart, R. R., 1984, Vertical seismic profiling, Part B: Advanced concepts: Geophysical Press, 1984.
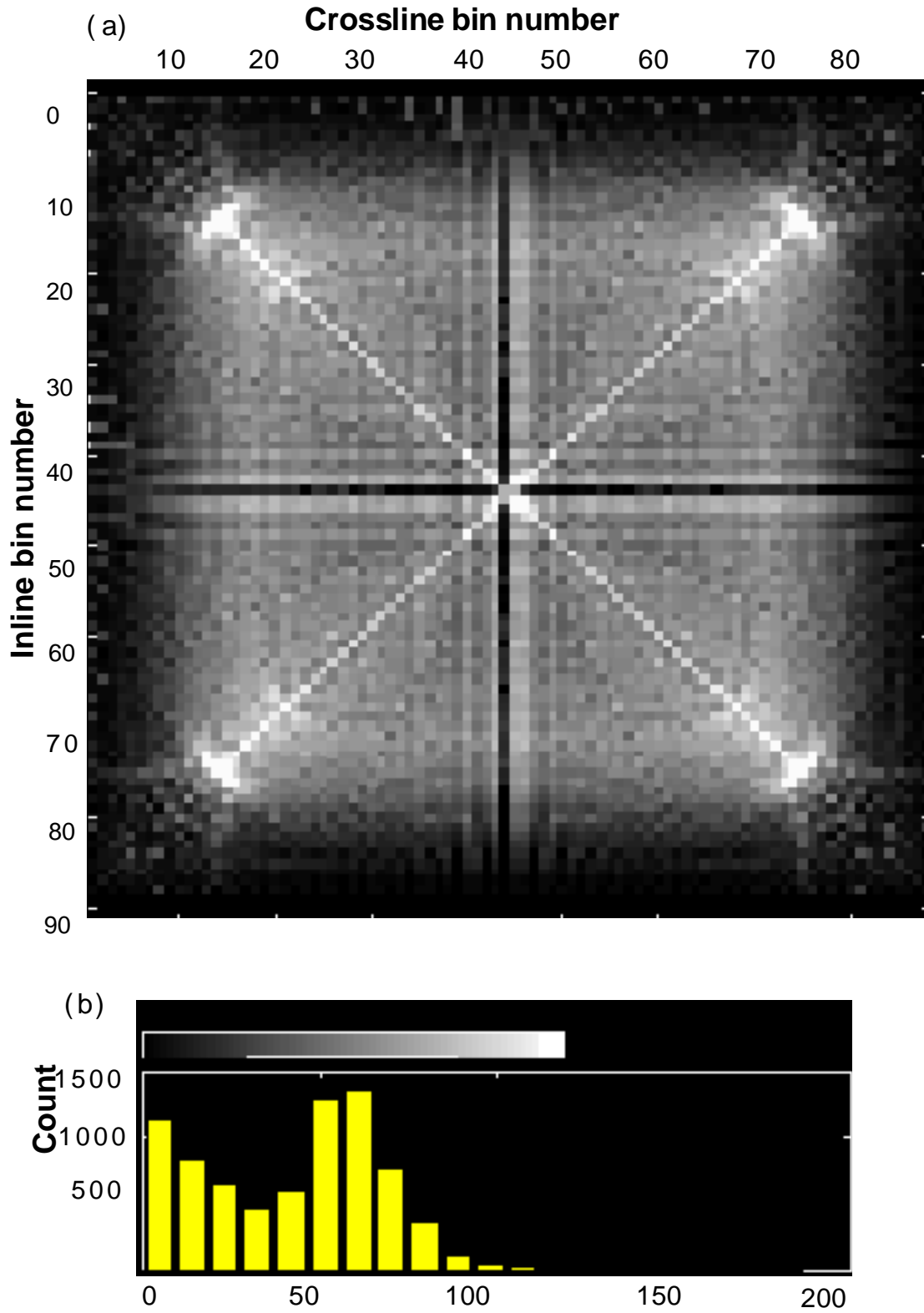
(a)

Crossline bin number

(b)

FIG. 6 Bin fold distribution display of second layer of the full shot and receiver dataset of model A. The receiver interval is 50 m; shot interval is 40 m; bin size: 15*15 m. (a): Areal fold distribution, (b): histogram of fold distribution.
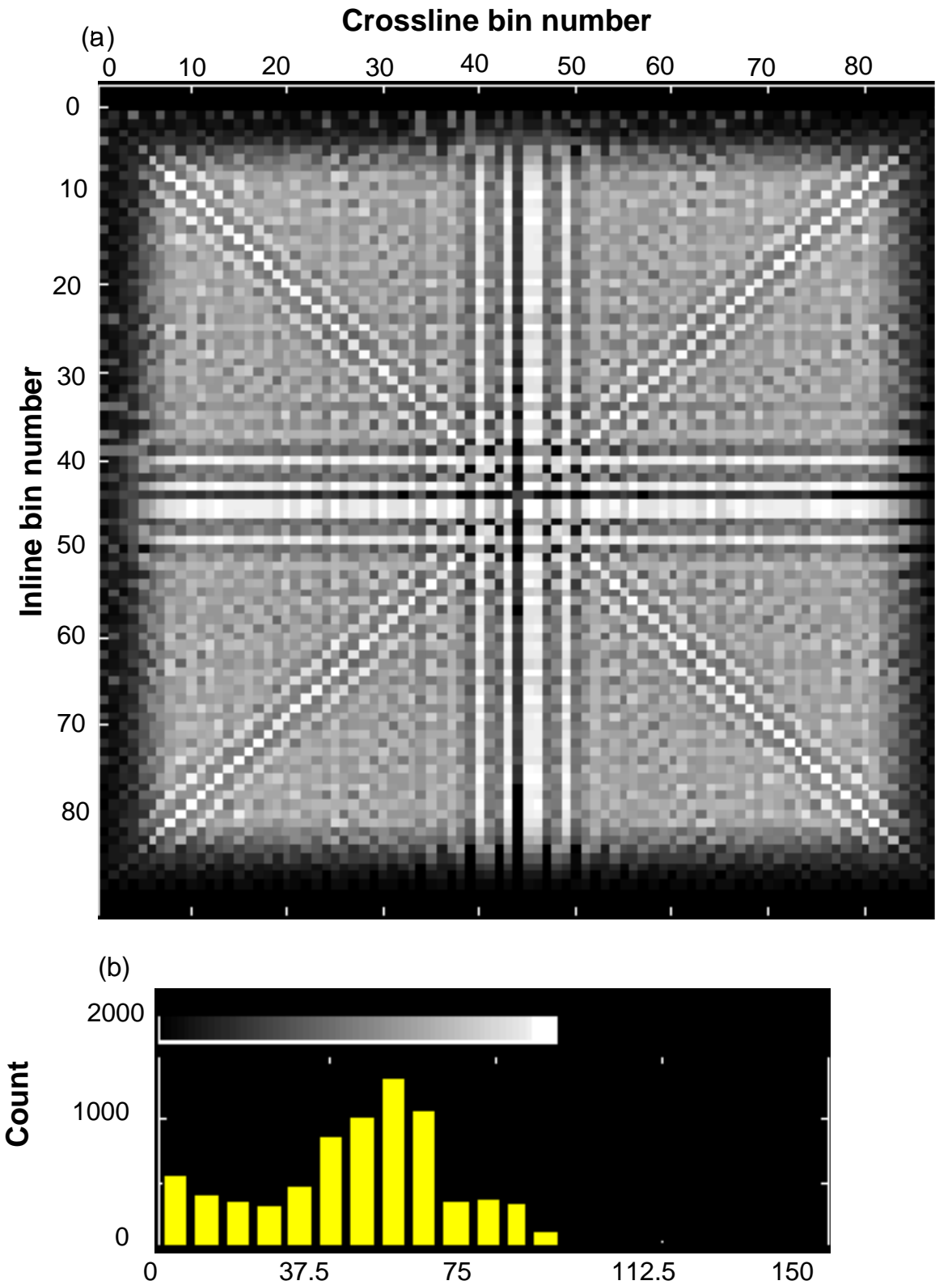
FIG. 7. Bin fold distribution display of the third layer for the full dataset of model A. (a): Areal fold distribution, (b): histogram of fold distribution.
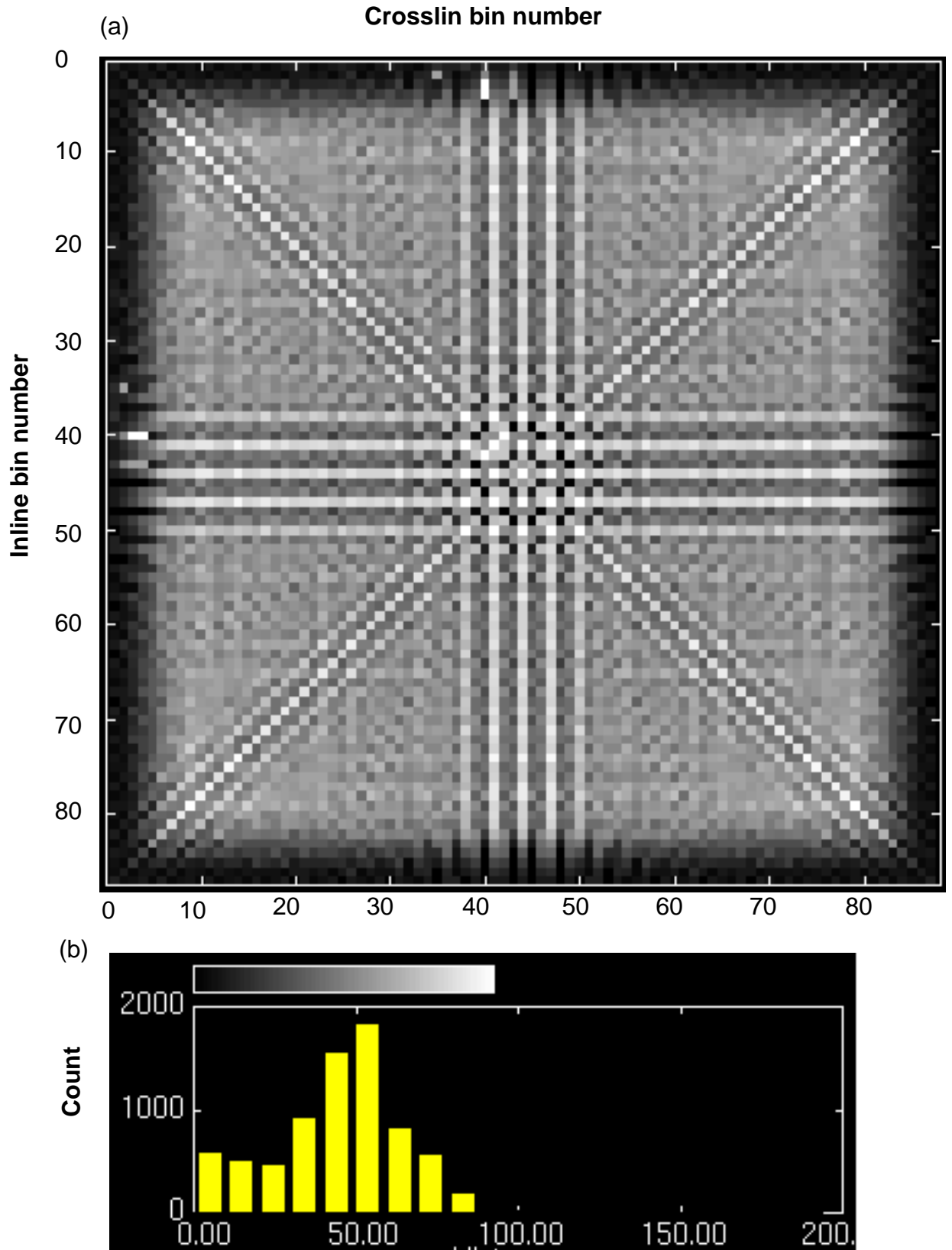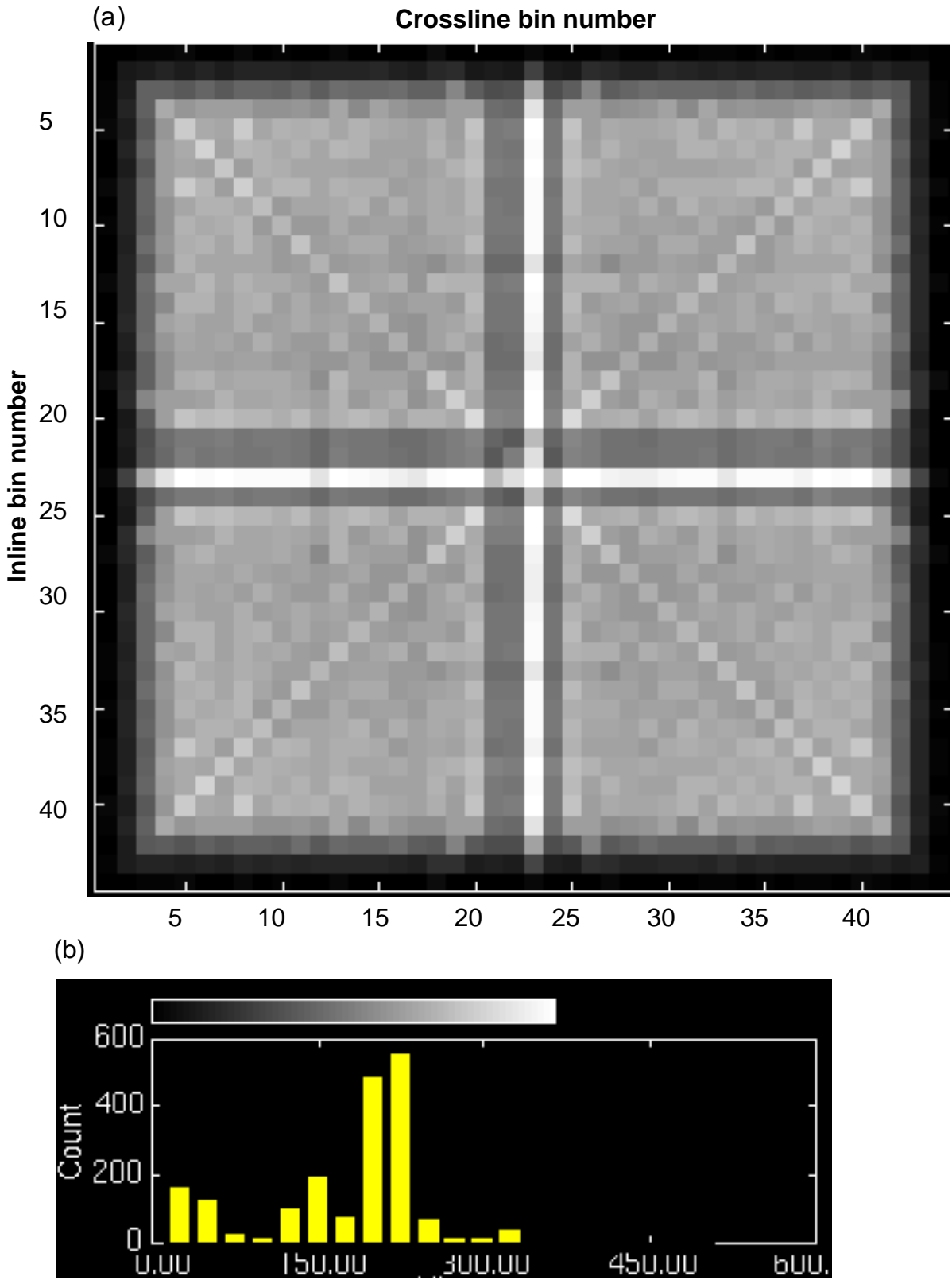
(a)

Crosslin bin number

(b)

FIG. 8. Bin fold distribution display of third layer of full dataset of model A, the receiver interval is 50m, shot interval: 40m, bin size 15 *15 with a bin shift of 7.5 m towards north and west direction. (a): Areal fold distribution, (b) histogram of fold distribution

(a)

Crossline bin number

(b)

FIG. 9. Bin fold distribution display of third layer of full dataset of model A. (a) : Areal fold distribution, (b): histogram of fold distribution. Receiver interval 50 m, shot interval: 40m, bin size 30*30 m.

(a)

Crossline bin number

(b)
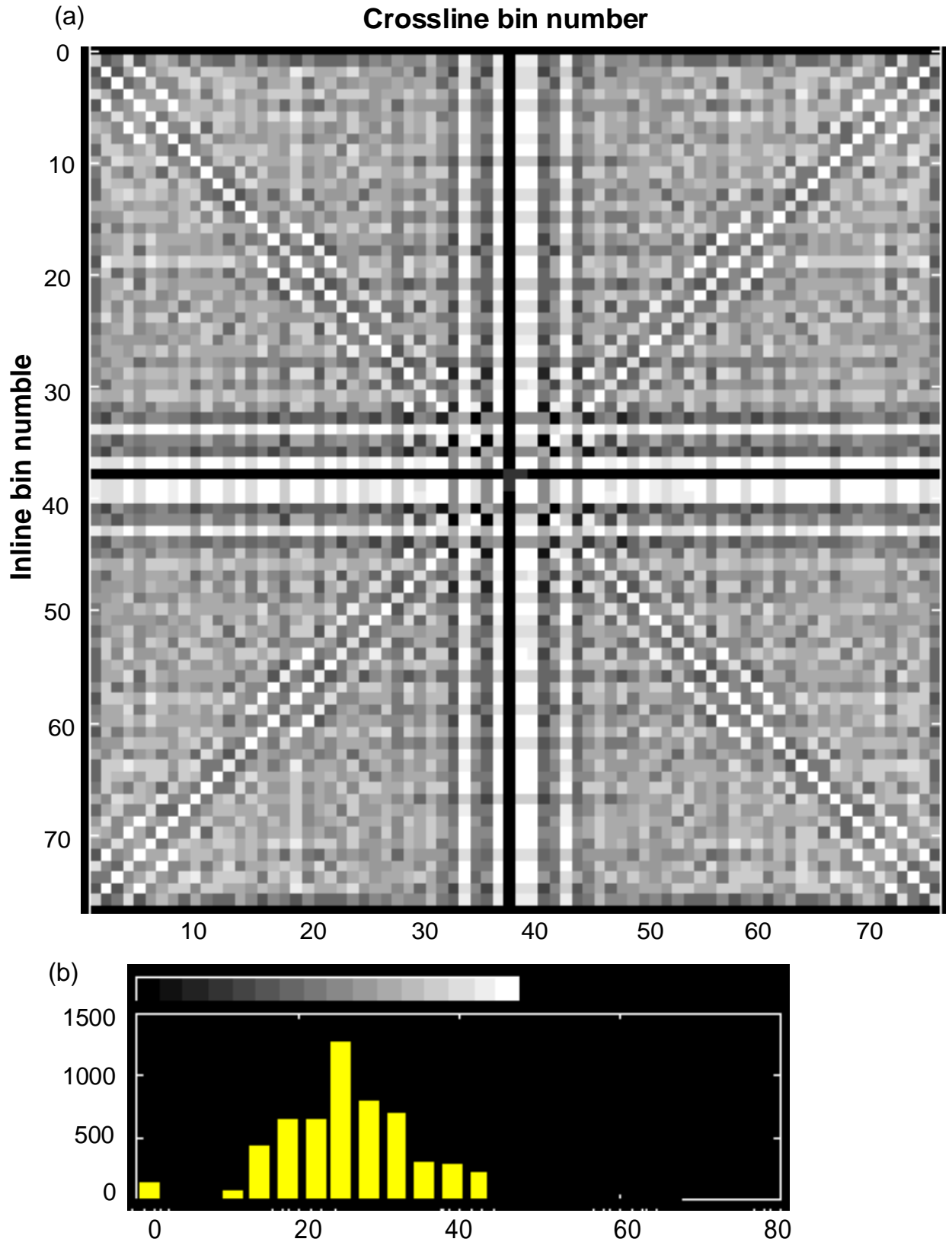
FIG 10. Bin fold distribution display of the third layer of model A. All receivers, with a receiver interval of 50m, 15 shots with an interval of 80m, bin size: 15*15m. (a): Areal fold distribution, (b): histogram
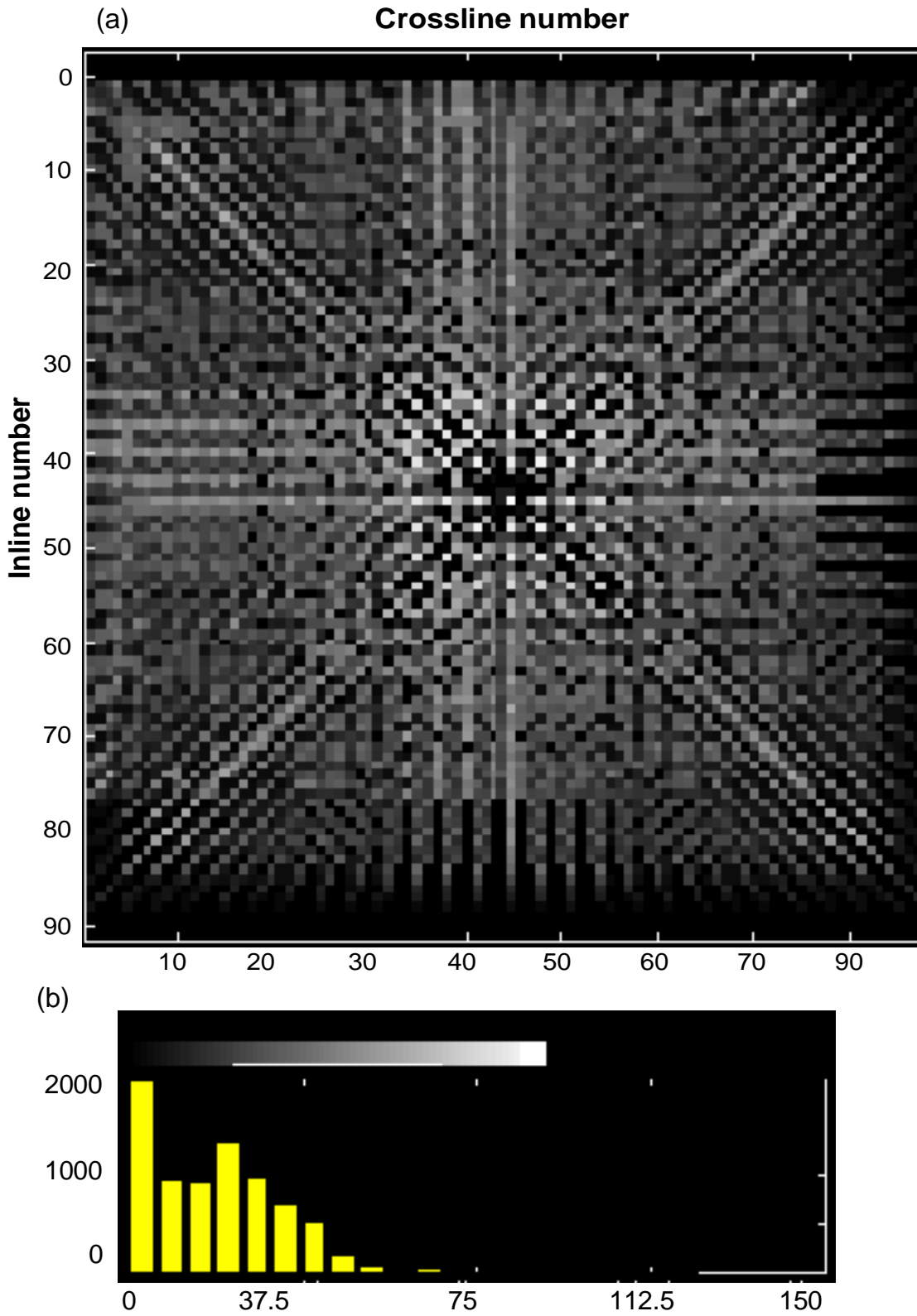
(a)

Crossline number

(b)

FIG. 11. Bin fold distribution using one quarter of the surface receivers. Receiver interval of 100m , 30 shots with a 40 m interval. The bin size is15*15m. (a): Areal fold distribution; (b): histogram of fold distribution.

Input preprocessed data

↓

Calculate RMS velocity and two-way
traveltime by using known velocities

↓

Calculate NMO time

↓

Apply NMO correction

↓

Stretch mute at far offset
of shallow layers

↓

Output NMO corrected trace
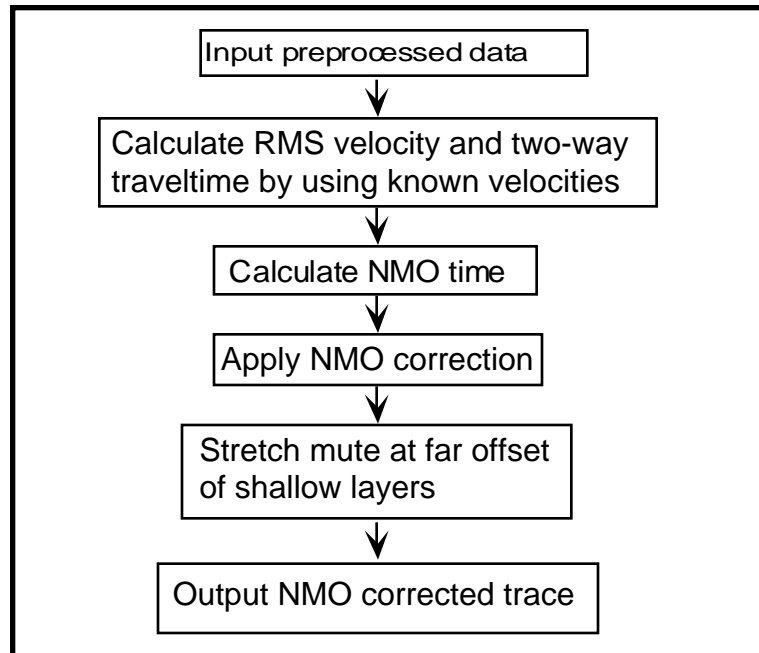
FIG. 12. 3-D VSP P-P wave NMO correction flowchart

Input NMO applied dataset

↓

Calculate maximum coverage for
all offset (azimuth)

↓

Define bin grid and azimuth in xy plane

↓

Calculate RMS velocity and raypaths
traveltime

↓

Calculate CRP coordinates in xy plane
at each depth point for each input trace

↓

Binning CRP in xy plane for each depth
point and calculate bin fold

↓

Stack data and output
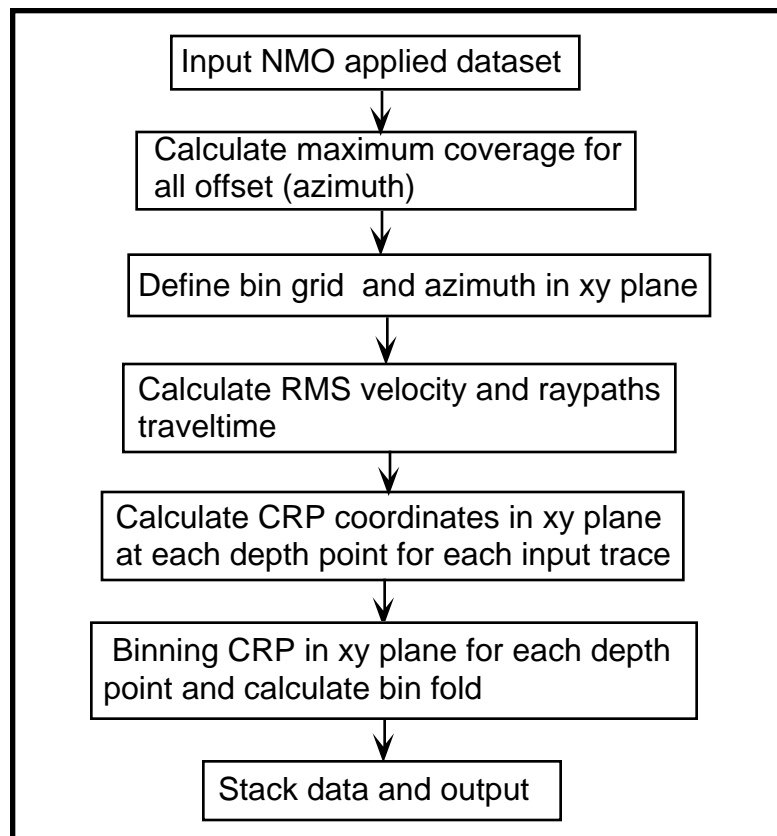
FIG. 13. 3-D VSP P-P wave binning and stacking flowchart
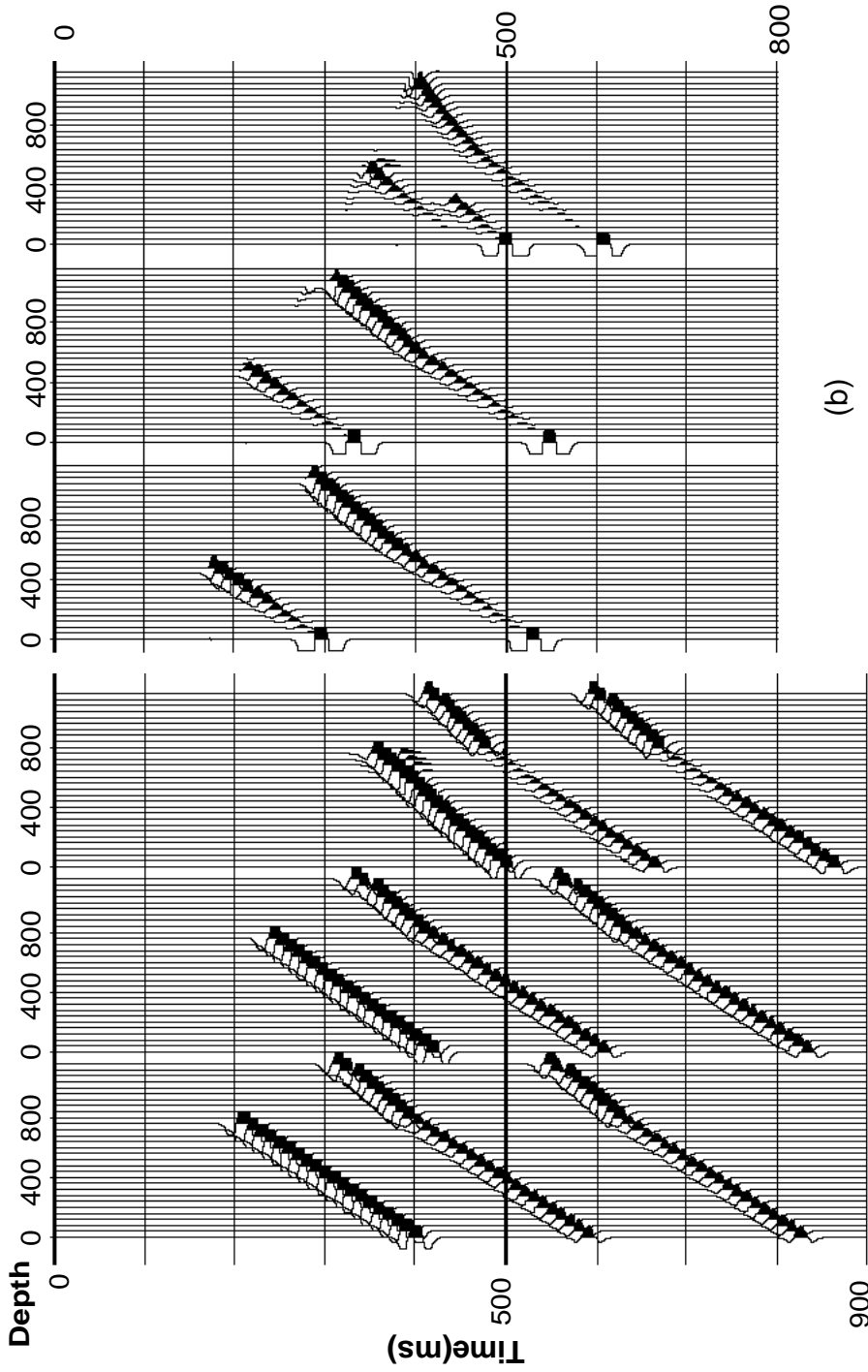
FIG.14 Receiver gather of upgoing wavefield located at east-west 1500m, north-south 1500m,2000 m, 2700 m from left to right.
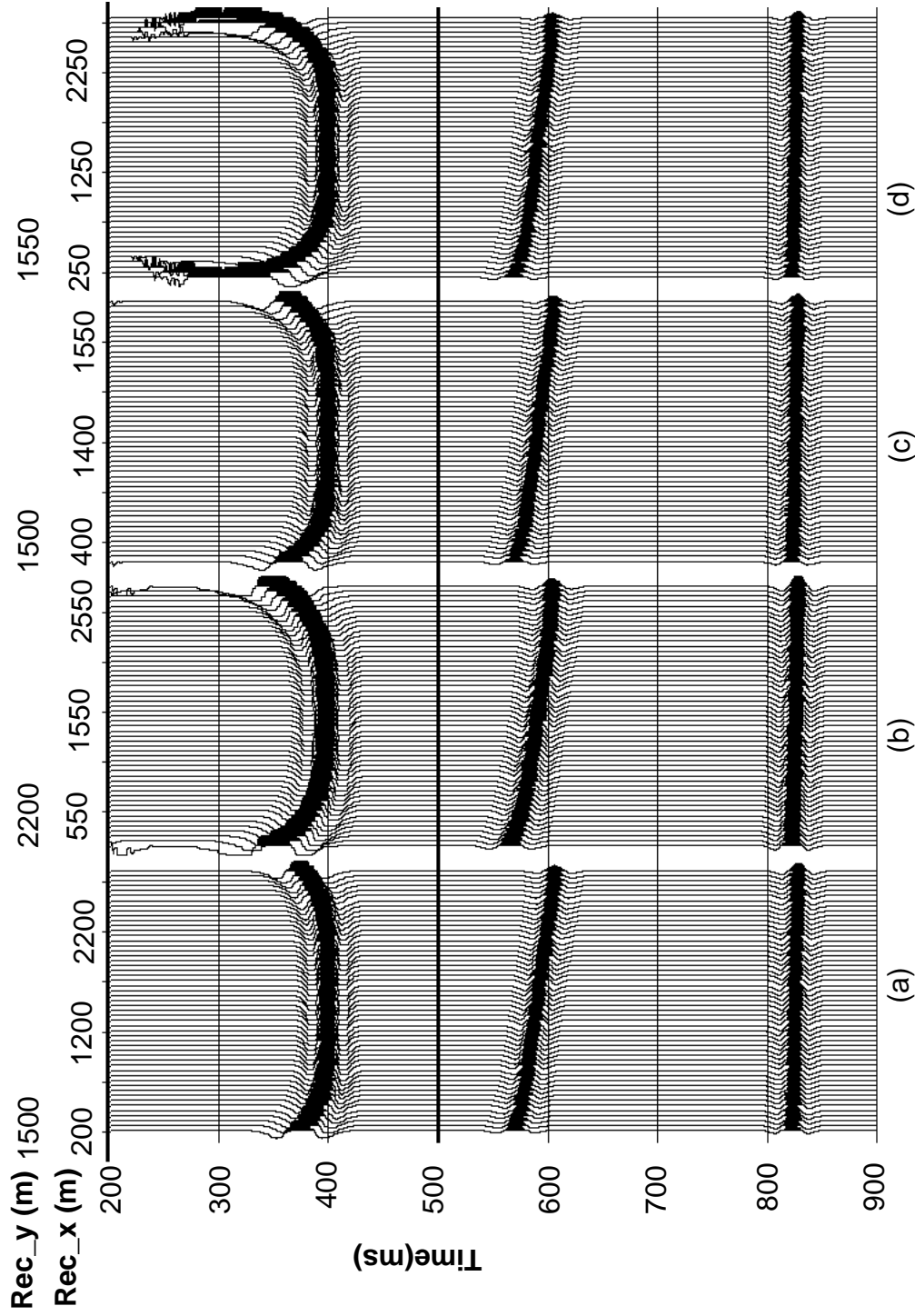(a): model A; (b): model B

FIG. 15. The NMO applied section on dataset A in common shot gather. Shot depth at : (a): surface; (b):surface; (c):120 m; (d): 320 m.
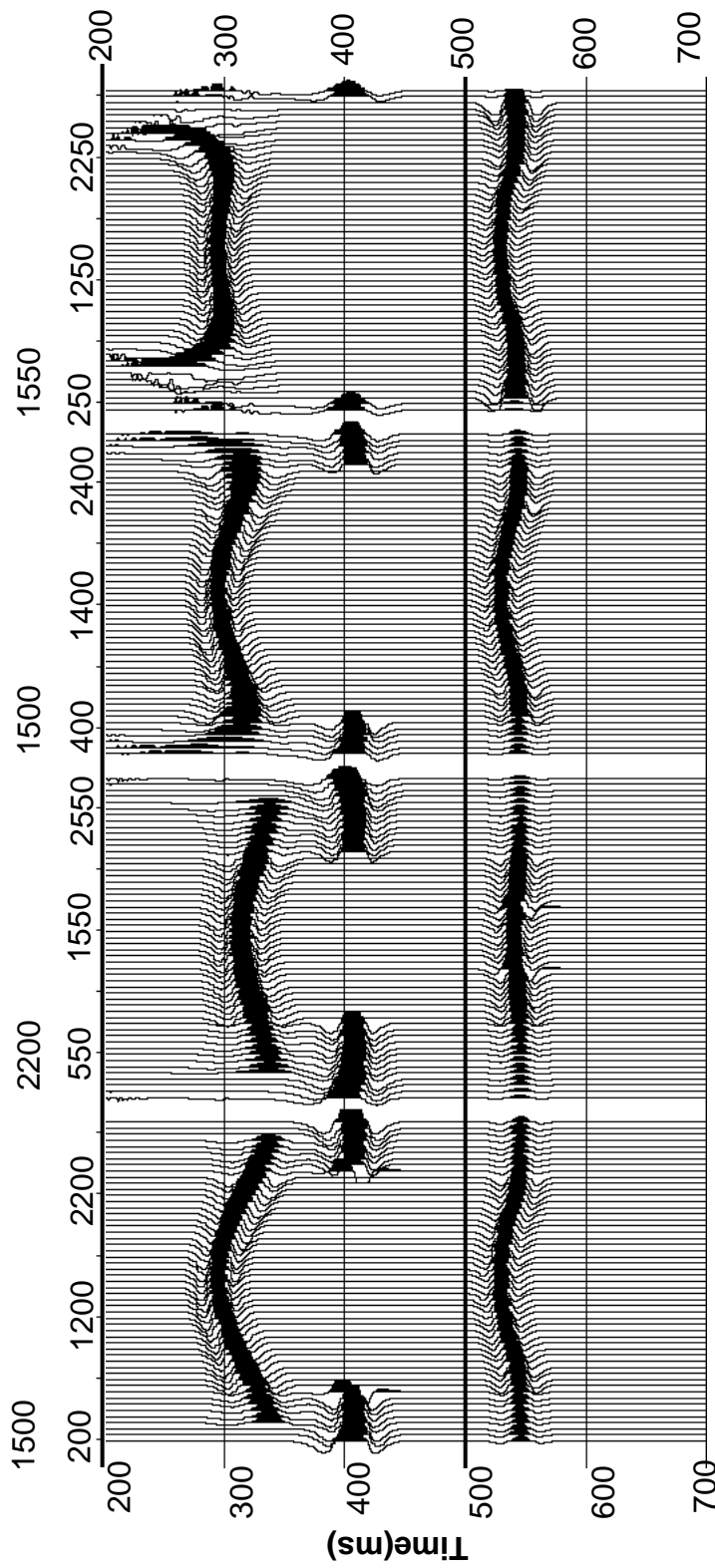
FIG. 16. The NMO applied section on dataset B in common shot gather. Shot depth at (a):surface; (b):Surface; (c): 120 m; (d): 320 m
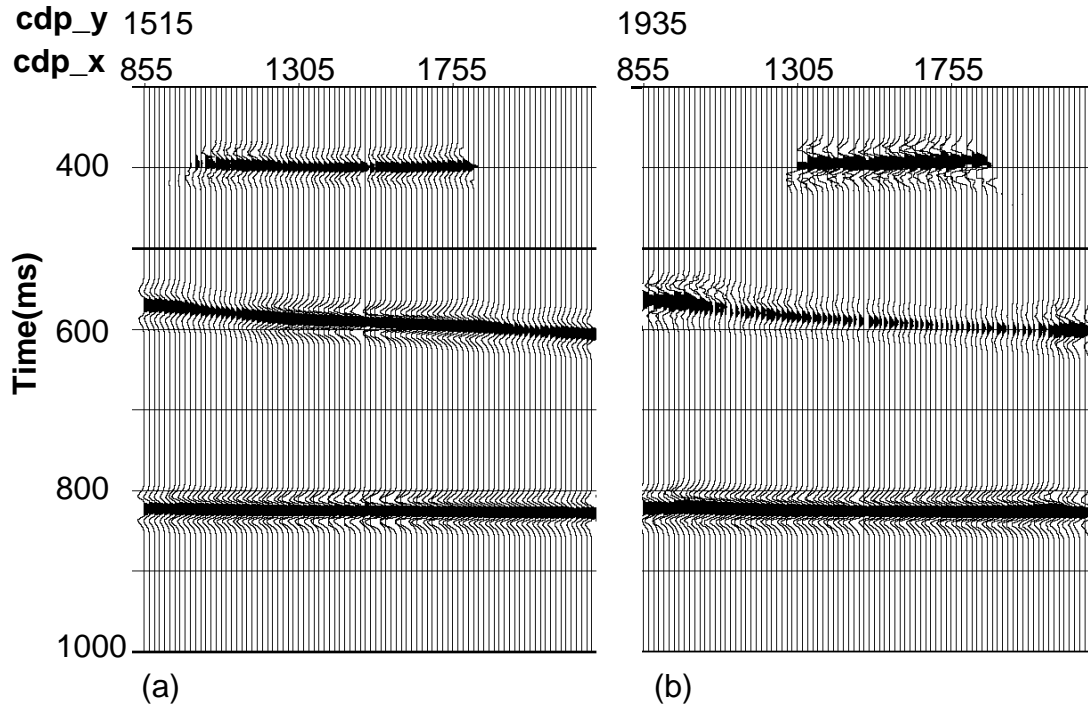
cdp_y 1515   1935

cdp_x 855   1305   1755   855   1305   1755

FIG. 17. The binning and stack section of model A. (a): the Inline section at cdp_x 1530 m, (b):the Inline section at cdp_y 1935 m.

cdp_y 1530   2025
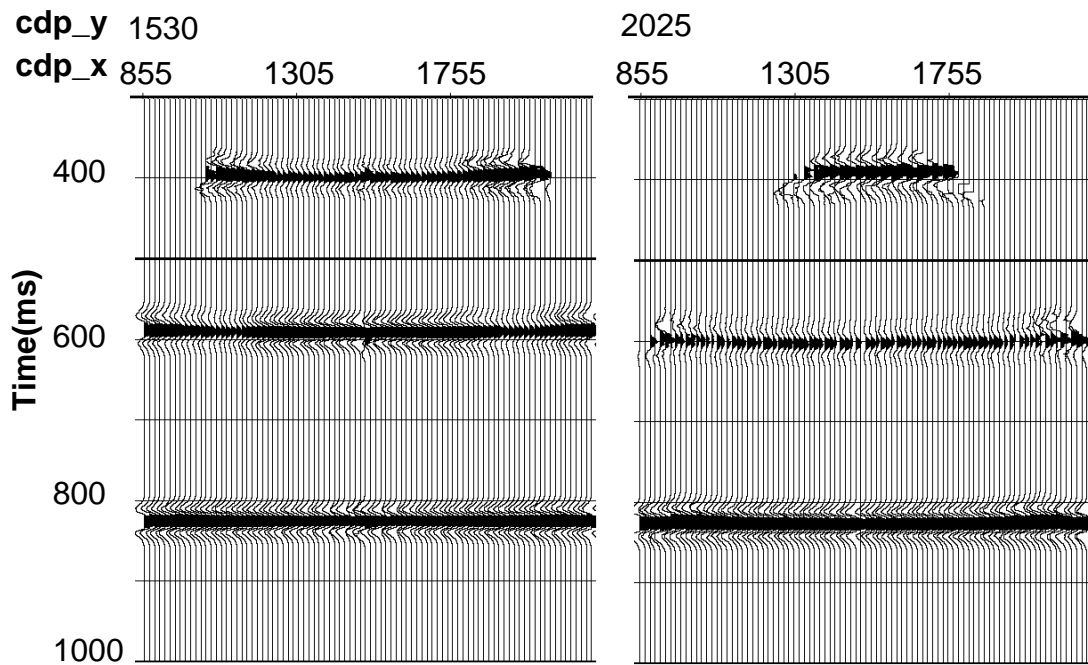
cdp_x 855   1305   1755   855   1305   1755

FIG. 18. The binning and stack section of model A. (a): the Cross-line section at cdp_x 1530 m, (b): the cross-line section at cdp_x 2050 m.
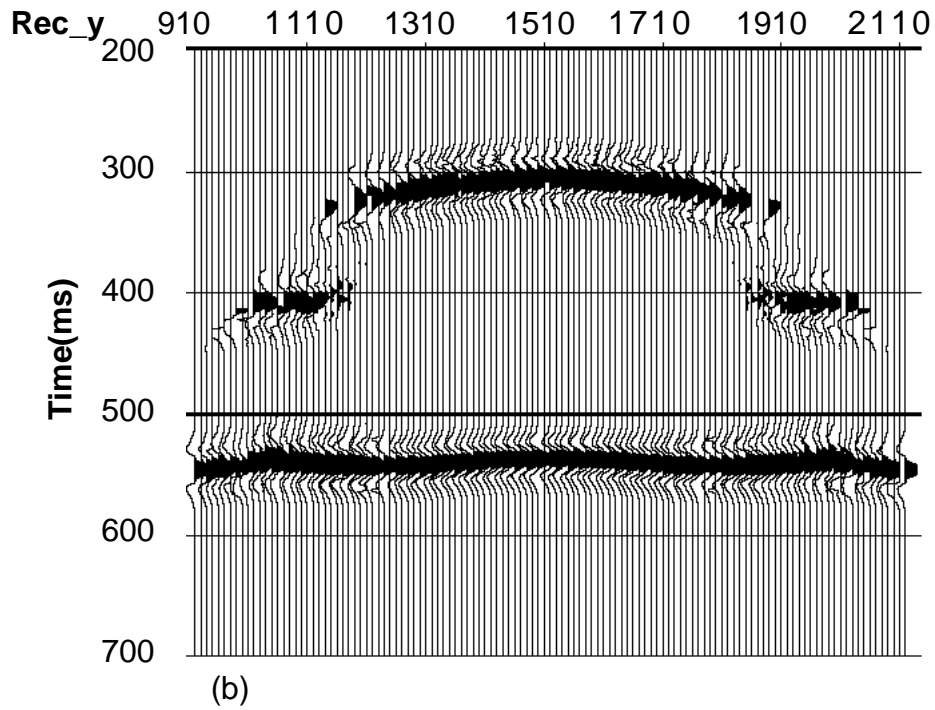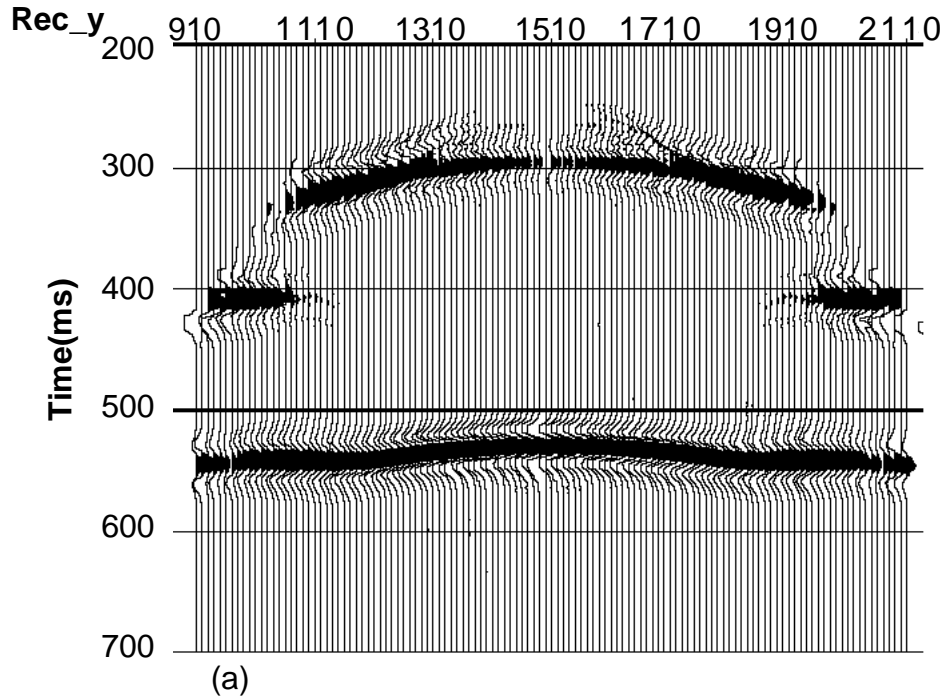
FIG.19. The binning and stack section of model B. (a): At near offset cdp_x 1515 m; (b): At far offset cdp_x 1230 m.